SCIENTIFIC REPORTS

OPEN

SUBJECT AREAS:
POROUS MATERIALS
METAL-ORGANIC FRAMEWORKS
BATTERIES
SYNTHESIS AND PROCESSING

Received
4 March 2013

Accepted
17 May 2013

Published
3 June 2013

Correspondence and requests for materials should be addressed to R.Z. (rzou@pku.edu.cn)

Facile preparation of hierarchically porous carbons from metal-organic gels and their application in energy storage

Wei Xia, Bin Qiu, Dingguo Xia & Ruqiang Zou

College of Engineering, Peking University, Haidian District, Beijing 100871, P. R. China.

Porous carbon materials have numerous applications due to their thermal and chemical stability, high surface area and low densities. However, conventional preparing porous carbon through zeolite or silica templates casting has been criticized by the costly and/or toxic procedure. Creating three-dimensional (3D) carbon products is another challenge. Here, we report a facile way to prepare porous carbons from metal-organic gel (MOG) template, an extended metal-organic framework (MOF) structure. We surprisingly found that the carbon products inherit the highly porous nature of MOF and combine with gel's integrated character, which results in hierarchical porous architectures with ultrahigh surface areas and quite large pore volumes. They exhibit considerable hydrogen uptake and excellent electrochemical performance as cathode material for lithium-sulfur battery. This work provides a general method to fast and clean synthesis of porous carbon materials and opens new avenues for the application of metal-organic gel in energy storage.

Carbon materials have long been widely used, such as graphite for pencil, carbon blacks for conducting additives, activated carbons for mask and carbon fibers for construction materials. Among them, porous carbons are gaining increasing attention due to the potentials to address the present energy and environment issues. These materials, associated with the advantages of high thermal and chemical stability, large surface area, light weight and large physisorption capacity, have been employed in hydrogen storage[1,2], pollutants adsorption[3], electrode materials[4], and catalyst supports[5]. Varieties of methods have been developed to prepare porous carbon, such as polymer carbonization[6–8], template method[9], chemical vapour decomposition[10], segregation reaction[11], and chemical or physical activation[12]. Among them, template approach is an efficient way to prepare porous carbon materials with tunable structures and pore textures[13]. Traditional inorganic materials zeolite and silica are known templates for casting porous carbon. However, this method is costly, complicated and always involves in highly toxic substances, which hinders its application in large scale production.

Very recently, preparing porous carbon materials or metal oxides directly from metal-organic frameworks (MOFs) or porous coordination polymers (PCPs) has emerged as a novel strategy and raised broad interests[14–30]. MOFs, built by metal ions and organic ligands, have attracted considerable attention due to their tunable pore size and functionality, high surface area and high thermal stability[31]. Motivated by these properties, Xu's group firstly reported the use of MOF-5 template to produce porous carbon, which exhibits high surface area, large hydrogen storage capacity and high performance as electrode materials for supercapacitor[14]. Other templates such as ZIF-8, IRMOFs, Al-PCP, and IRZIFs were also successively applied. Typically, carbon precursor, furfuryl alcohol (FA), was introduced into the pores of porous MOFs. After polymerization and carbonization, hierarchically porous carbon products were achieved, of which the micropore/mesopore/macropore ratio depends on the precursor introduction method (incipient wetness or vapor method) and carbonization condition[14,16]. Some researchers also confirmed that additional carbon sources are not necessary in producing MOFs-templated carbons with high surface area owing to the large carbon content in MOFs, which makes the procedure easier[18,22–24]. This strategy shows an effective way to produce porous carbon. However, there are still some aspects should be noticed. The most obvious part is that all the works are based on MOFs or PCPs which are subject to costly and time consuming building-up processes. Organic solvents such as N,N′-dimethylformamide (DMF) and N,N′-diethylformamide (DEF) are often used in preparing MOFs or PCPs. These solvents are toxic and teratogenic reagents that need special actions to dealing with. Thus the application of this method in industry is limited[32]. In addition, though some reports showed that porous carbon products with superhigh surface area could be achieved, these values drop drastically when scaled up[23].

On the other hand, metal-organic gels (denoted as MOGs) are a new type of extended MOF structure[33]. These compounds are fabricated on the basis of coordination complexes, and assembled to form 3D networks by hydrogen bonding, π-π stacking and/or van der Waals attraction[34]. Compared to MOFs, MOGs suffers from the poor crystallinity, and their structure remains uncertain, but they also show great potential in catalysis, gas storage and separation due to their abundant Lewis acid sites and porous gel structures[35]. They share the high thermal stability as well. Notably, MOGs have their particular characters. The synthesis condition for these compounds are quite gentle with low temperatures, sometimes even at room temperature, neutral condition and short reaction times. In addition, the solvent used is the relatively cheap and clean ethanol, which greatly reduces the cost and attention that were paid. However, the use of MOGs as carbon precursor has never been reported. The similarity of MOGs to MOFs prompted us to think that MOGs may also perform well in fabricating nanoporous carbon.

The present paper describes a general way to prepare nanoporous carbon materials from MOGs. We obtained two types of carbon products by simple varying the structure of the gel precursors. Carbonizing the xerogel precursors leads to nanoporous carbon materials with unexpectedly high surface area and hydrogen storage capacity. Alternatively, carbon monoliths with quite large pore volume can be achieved through the metal-organic aerogels (MOAs). A hierarchical structure with micropores, mesopores and macropores was found in this type of carbon products which are highly suitable for sulfur confinement matrix in Li-S battery.

Results

The target MOGs were first prepared by mixing aluminum nitrate and 1,3,5-benzentricarboxylic acid in ethanol solutions. After only 1 h reaction in sealed Teflon containers at 120°C, light yellow wet gels were obtained. Then the as-synthesized gels were dried in air or by supercritical CO_2, resulting in MOXs and MOAs, respectively. The two gels were then carbonized to construct the target porous carbon products, named as MOX-C and MOA-C, respectively.

The original wet gels have a hierarchical architecture which is presented in Figure 1. Specifically, the primary stage is 1,3,5-benzen-

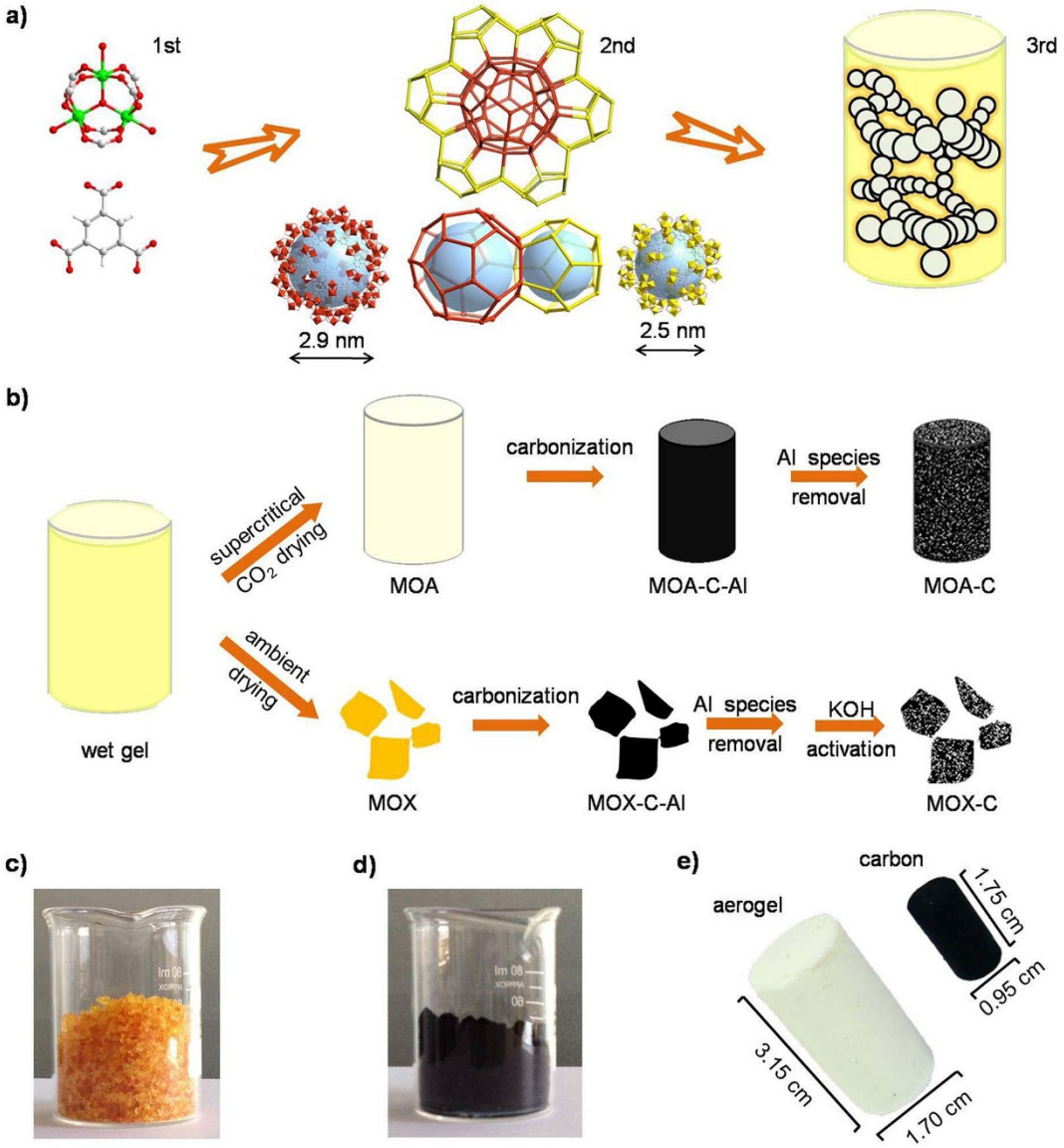

Figure 1 | Fabrication of porous carbon materials from Al-based metal-organic gels. (a) Schematic illustration of the gel structure, (b) typical synthesis procedure of the porous carbon products, (c, d) photographs of as-made xerogels (bulk density: 0.5612 g cm^{-3}) and their derived carbon products MOX-C (0.1185 g cm^{-3}), and (e) photograph of an integrate aerogel monolith (0.1189 g cm^{-3}) and its derived carbon product MOA-C (0.0952 g cm^{-3}).

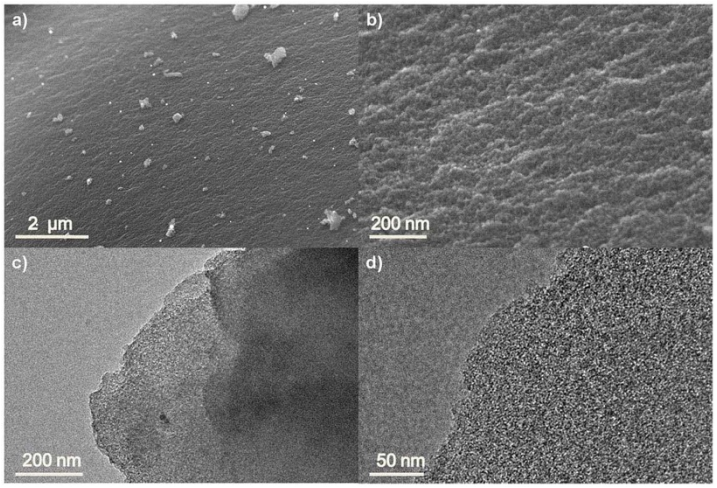

Figure 2 | **(a, b) SEM and (c, d) TEM images of MOX-C.**

tricarboxylic acid ligands and metal clusters built from the actahedrally coordinated Al(III) with four carboxyl oxygen atoms. These basic building blocks will assemble into the secondary stage, namely nanoparticles of MOF substructure. Powder X-ray diffraction (PXRD) reveals a close relationship to the MIL-100(Al) crystal that bears the Zeolite MTN topology with two types of cages, small cages and large cages (Figure S1). The tertiary structure is the 3D network from the interconnected nanoparticles. Mesopores (2 $\sim$ 50 nm) and macropores ($>$ 50 nm) were formed as the interspaces among the packed particles. But, these macropores crash in the ambient dried xerogel samples due to the capillary forces during the drying process. However, the macropores remain intact after supercritical CO_2 treatment. This drying method has been proved to be the most prominent procedure in removing solvent from the pores while bringing the least changes to the original structure[36]. The difference is obvious. We can see that the as-synthesized xerogels are small deep yellow particles, while the aerogel products are superlight integrated yellowish columns that keep the shape of the wet gels. Figure S2 shows that a piece of common note paper can easily hold a MOA monolith. The different colors in xero- and aerogel indicate the different microstructures[37], especially the pore sizes which were further revealed by SEM and TEM images (Figure S3, S4). The MOA samples have a higher degree of porosity and looser structure than MOX. Macropores were only found in MOA samples, which leads to their super light nature and lighter color.

The morphologies of the gel precursors play a critical role in shaping the structures of their derived carbon products. Carbons from these gels possess the similar microstructures to the gel precursors (Figures 2, 3). For MOX-C samples, no detectable macropores were observed. Whereas, for the MOA-C products, interestingly, though they are much smaller than the aerogel precursors due to the heat treatment, they keep the high degree of macroporosity. SEM and TEM images clearly show the porous carbon matrix that consists of interconnected nanoparticles.

These results are highly consistent with the nitrogen sorption analysis (Figure 4). Typical Type-IV isotherms are found in the MOX-C as well as the MOX. There are hysteresis loops between the adsorption and desorption branches, implying the mesoporous

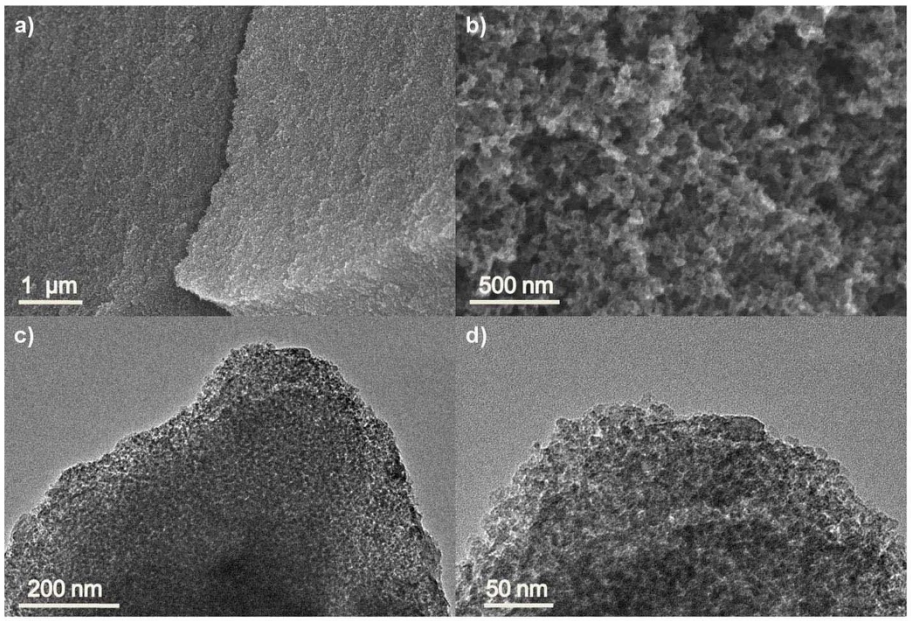

Figure 3 | **(a, b) SEM and (c, d) TEM images of MOA-C.**

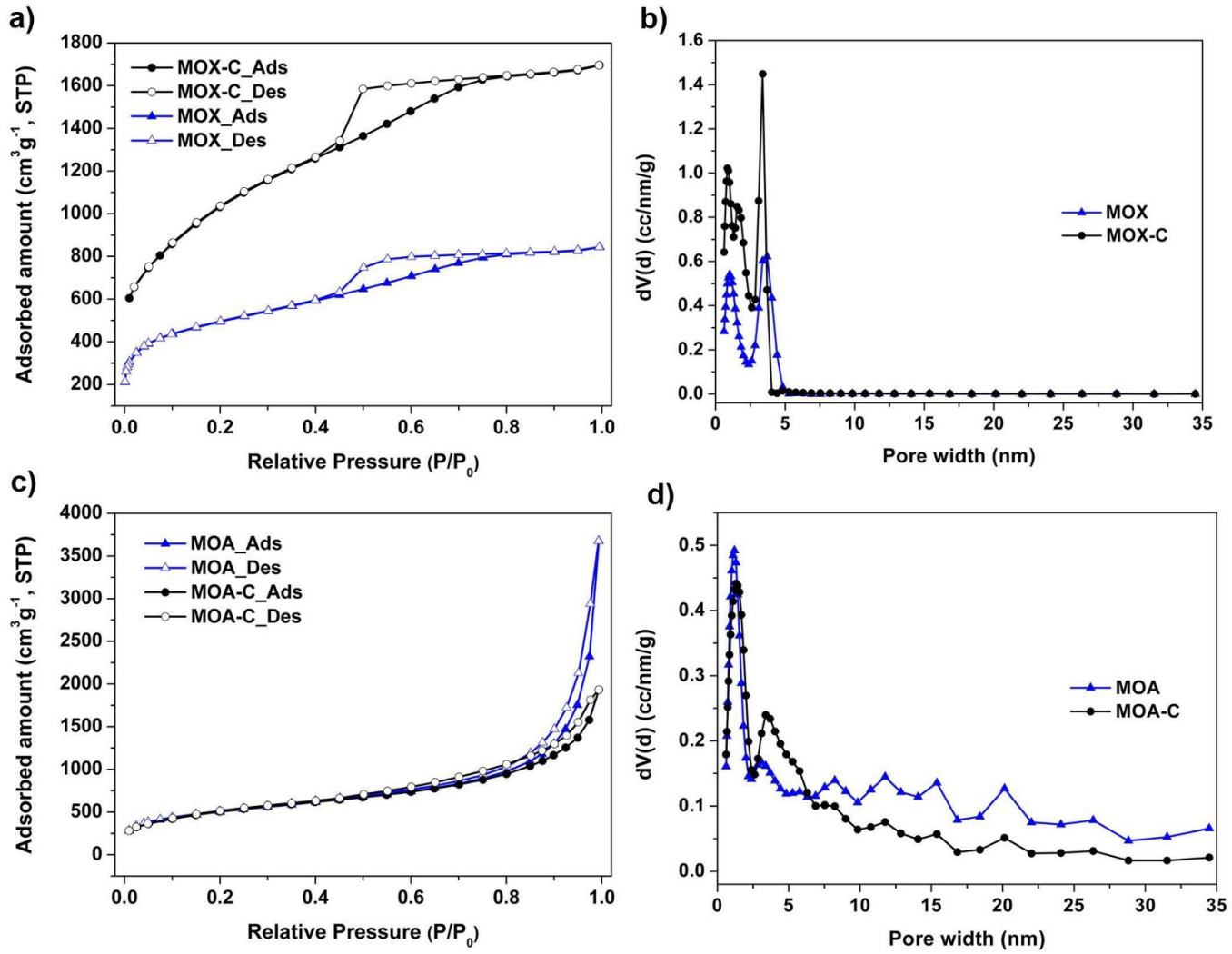

Figure 4 | N_2 **sorption isotherms at 77 K and pore size distributions of (a, b) MOX and MOX-C, and (c, d) MOA and MOA-C.**

character in both samples. MOA and MOA-C display the Type-II isotherms with the vertical tails at around 1.0 relative pressure, which reveals the macroporosity in the samples[14]. All the carbon products and the gel precursors display considerable N_2 adsorption at low pressure. This can be attributed to the presence of microporosity in all the samples. The details of the pores are displayed by the pore size distributions (PSD) based on QSDFT equilibrium model. The results show that the MOX and MOX-C have narrow PSDs mainly focused on 1.0 and 3.4 nm. The MOA and its derived carbon products exhibit broader PSDs from micropores to large mesopores. Note that they display the similar PSDs to xerogels and their derived carbon samples at the low range. These pores arise from the MOF MIL-100(Al) like sub-structure.

Unexpectedly, a quite high Brunauer-Emmett-Teller (BET) surface area of 3770 m^2g^{-1} and pore volume of 2.62 cm^3g^{-1} were found for the MOX-C. To the best of our knowledge, these figures, especially the BET surface, are close to the highest value for template carbon materials up to date (e.g., ZTC, PFA-P7)[38,39]. Table 1 summarized the textural properties of the MOF derived carbon materials from recent works, we can see that the surface area of MOX-C is much higher than most MOF derived carbon materials. As a bulk material, the MOA-C sample from this work displays a very high surface area calculated to be 1820 m^2g^{-1}. The pore volume is found to be an astonishing 3.22 cm^3g^{-1}, which is among the highest values for the the porous carbon materials.

Table 1 | Summary of the texture parameters of MOF derived carbons

Sample	S_{BET}[a] (m^2g^{-1})	V[b] (cm^3g^{-1})	Ref
NPC	2872	2.06	14
WMC	2587	3.14	15
NPC_{530}	3040	2.79	16
MC	1812	2.87	17
C1000	3405	2.58	18
CNF	90	0.23	19
Al-PCP-FA	513	0.84	20
BF-1000	1131	0.69	21
IRMOF-1	3447	1.45	22
PCP-800	5500	4.40	23
Z-1000	1110	0.62	24
6c	1820	1.84	25
C-70	1510	1.75	26
MOX-C	3770	2.62	This work
MOA-C	1820	3.22	This work

[a] S_{BET}: Specific surface area calculated by the Brunauer-Emmett-Teller (BET) method. [b] V: pore volume at relative pressure of $P/P_0 = 0.995$.

PXRD for these samples are shown in Figure S6. There are two broad peaks at $2\theta = 27^\circ$ and 50°, corresponding to the diffractions of (002) and (004) planes of turbostratic carbon[40]. The broad peaks indicate the amorphous nature of the carbon products that consists of small domains assembled by disordered graphene sheets. Notedly, for the MOX-C sample, there is no obvious peak at $2\theta = 27^\circ$. This is because the MOX-C samples had experienced the KOH activation, which has been reported to reduce the aligned structural domains in carbon materials while enhancing the microporosity[2]. Raman spectroscopy was combined to investigate the carbon structure (Figure S7). The spectra exhibited the D peak at 1342 cm^{-1} and the G peak at 1590 cm^{-1}. In general, the D peak arises from the disordered carbon structure[23]. As the defects in the sp^2 lattice structure increase, the intensity of the D peak increases. The ratio of the two peaks' intensity I_G/I_D has been used to evaluate the graphitization degree. A lower I_G/I_D value indicates a lower graphitization degree. The I_G/I_D value of MOX-C and MOA-C are found to be 1.03 and 1.09, respectively, which further confirm the lower degree of graphitization for MOX-C sample. This result is coincides with the PXRD patterns. In fact, TEM image in Figures S8, S9 provides a direct vision. Nanometer-sized disordered graphene sheets were found in the MOA-C , but for the MOX-C samples, such texture was not observed.

Discussion

Motivated by the high surface areas and unique porous structures of the carbon products, we explore them as candidate media for hydrogen storage. Hydrogen sorption measurement was conducted at 77 K up to 1 atm by volumetric method. The xero- and aerogel precursors were also characterized for comparison. The isotherms for these samples are showed in Figure 5a. All of them display reversible hydrogen uptake behaviours as no hysteresis appears between the adsorption and desorption branches. The H_2 uptake capacities of the carbon samples are higher than the gel precursors. For MOA-C and the gel precursor MOA, although they have the similar BET surface areas and pore structures, the H_2 sorption abilities are quite different. MOA-C sample displays a much higher capacity than MOA, which may be due to the stronger interactions between hydrogen and carbon matrix than those between hydrogen and MOG. As expected, MOX-C sample, with the highest surface area and developed microporosity, shows the highest hydrogen storage capacity at ambient pressure. Remarkably, the value is as high as 2.98 wt%, which is comparable to the benchmark porous materials that have the best known performance (e.g., PCN-12: 3.05 wt%; TiC-CDC: 3.0 wt%; AC-900: 2.7 wt%)[41–43].The adsorption abilities for CO_2 and CH_4 were also investigated at 273 K (Figure 5b). Similar to their H_2 adsorption behaviours, MOX-C and MOA-C have the higher uptakes of CO_2 and CH_4 than those of gels, in which the highest CO_2 adsorption uptake was 117 cm^3g^{-1} for the MOX-C.

These carbon products also show a good potential as cathode materials for lithium-sulfur batteries since the carbon matrix will smooth over the electronic conductivity problem of sulfur. Meanwhile, the existence of micropores and high surface area will help to confine the soluble polysulfides, which are crucial issues in Li-S system[44,45]. The C/S composites as cathode materials were prepared by a two steps melt-diffusion strategy (see details in Experimental Section). No bulk sulfur was fond in the SEM image in Figure 6a. And the corresponding carbon and sulfur elemental maps clearly show the homogeneous distribution of sulfur in the framework of the carbon materials (Figures 6b, c). PXRD patterns in Figure S12 shows the obvious peaks corresponding to sulfur disappear after the MOA-C/S sample was heated at 300°C, which indicates sulfur impregnation in the pores and the lack of bulk crystalline sulfur on the outer surface. Pore-filling is further confirmed by N_2 sorption isotherms (Figure S13). A similar shaped curve to the MOA-C was acquired for the MOA-C/S samples. The isotherms locates in the lower position, which indicates a similar hierarchical pore structure but relatively

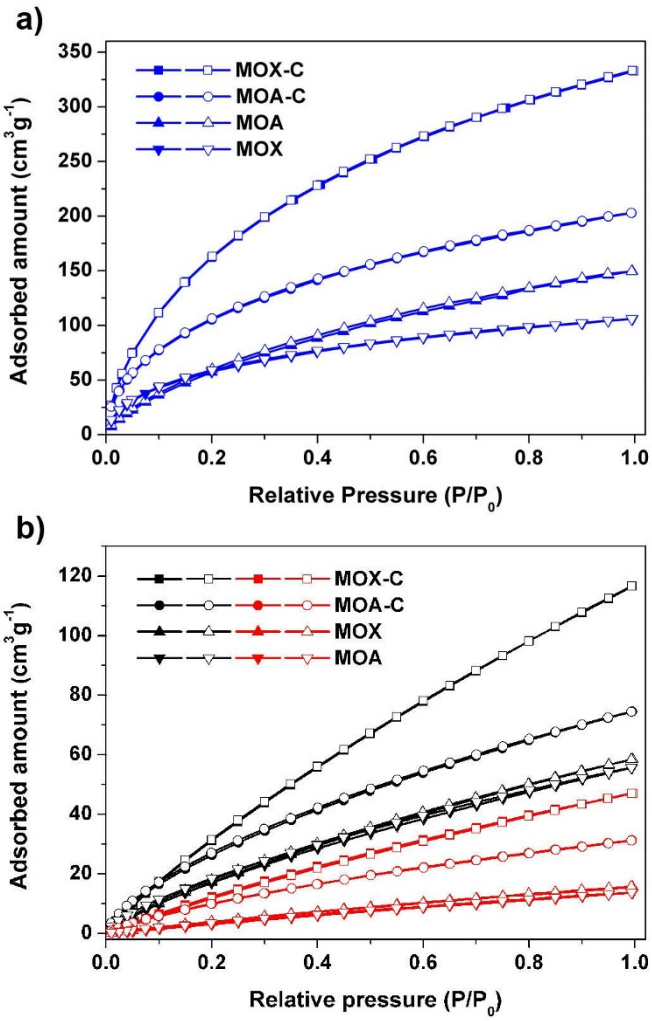

Figure 5 | Gas uptakes of MOX, MOA, MOX-C and MOA-C. (a) H_2 sorption isotherms at 77 K, (b) CO_2 (black lines) and CH_4 (red lines) sorption isotherms at 273 K. The solid and open symbols represent the adsorption and desorption branches, respectively.

lower specific surface area and pore volume due to the impregnation of sulfur in the pores. The BET specific surface area drops dramatically from the initial value of 1820 m^2g^{-1} to 200 m^2g^{-1}, while the pore volume decreases from 3.22 cm^3g^{-1} to 0.78 cm^3g^{-1}. The inset picture in Figure S13 clearly shows the great changes in pore size distributions before and after sulfur impregnation in the MOA-C. Most parts of the micropores were filled. The contents of sulfur in the MOX-C/S and MOA-C/S samples were confirmed by thermogravimetric analysis (TGA) (Figure S14): 30.3% and 50.9%, respectively. A parallel TGA test of pure sulfur was also conducted. Obviously, the C/S samples both start and end losing weight at higher temperatures compared to sulfur, which indicates a strong interaction between sulfur and the carbon matrix in the composites.

The charge-discharge profiles were recorded at a discharge rate of 400 mAg^{-1}. The capacity values in this paper are all based on the mass of sulfur. Figures 6d,e show the initial three cycles. They present typical C/S profiles with two plateaus at 2.0 V and 2.3 V. Both samples display very high discharge capacities but the MOA-C/S sample performed better. Considering the existence of common side reaction happened in the 1st cycle, we compare the capacities from the 2nd cycle. The MOA-C/S composites show an impressive discharge capacity of 1240 $mAhg^{-1}$ (74% of 1675 $mAhg^{-1}$ the theoretical value) at the 2nd cycle and the capacity remains at 1155 $mAhg^{-1}$ at the 3rd cycle. For the MOX-C/S samples, the figures are slightly

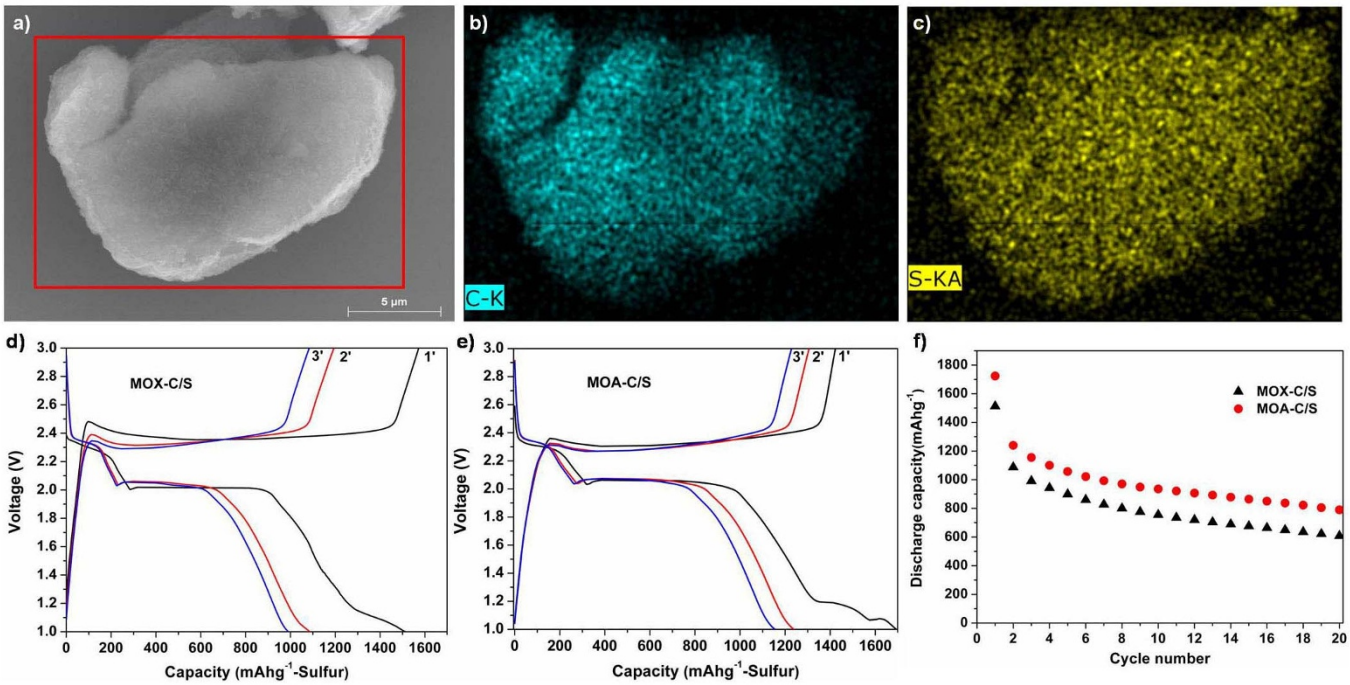

Figure 6 | (a) SEM image of MOA-C/S composite, (b, c) corresponding carbon and sulfur elemental maps, (d, e) charge-discharge profiles of MOX-C/S and MOA-C/S for the initial three cycles at a current density of 400 mAg^{-1}, and (f) discharge capacity of MOX-C/S and MOA-C/S versus the cycle numbers.

lower. That is, 1087 and 991 $mAhg^{-1}$ for the 2nd and 3rd cycle. Figure 6f shows the cycling performances of the composites. Obviously, MOA-C/S composites have the higher capacity and better cycling behaviour. This may be attributed to the hierarchical pore structure of the MOA-C, in which the macropores could work as reservoirs of electrolyte and the mesopores might act as transport paths while the micro- and mesopores could confine sulfur. Template-based porous carbons have been widely explored as platforms for energy storage, however, monolithic carbons with 3D penetrated pores are rare and in urgent need now[46]. Here, the MOA templated carbon, MOA-C, possessing the unique three dimensional structure with the high surface area, large pore volume and hierarchically porous structure, shows the good prospect in energy storage. However, we can see that the discharge capacity drops slightly as the cycle number increases, which is a common problem for Li-S batteries[44]. More work is on the way to improve the cycle performance.

In summary, we have for the first time applied metal-organic gels to prepare nanoporous carbon materials. We systematically study the influence of the gels structure to the derived carbon products. The results show that the xerogel derived carbon exhibits a very high surface area and hydrogen storage capacity while the aerogel derived carbon monolith has a hierarchical pore structure with micro-, meso- and macropores and quite large pore volume, which is quite suitable for Li-S batteries. This work provides a general method to fast and clean synthesis of porous carbon materials and open new avenues for the application of metal-organic gel based materials in energy storage. Due to the diversity of the MOGs composed from different metals and ligands, more pore textures tailorable carbon and other elements doped carbon materials could be anticipated. More work is in progress in our group.

Methods

Synthesis. The aluminum based metal-organic wet gels were firstly prepared by dissolving 1.42 g $Al(NO_3)_3 \cdot 9H_2O$ and 0.52 g 1,3,5-benzentricarboxylic acid (H_3BTC) in 18 mL ethanol under vigorous stirring at room temperature. The mixture was transferred to Teflon containers sealed in stainless steel vessels and heated at 120°C for 1 h. The resulting wet gels were placed in autoclave and subsequently dried with supercritical CO_2 to obtain monolithic aerogel samples. Xerogel products were prepared by drying the wet gels in an oven at 80°C. Then the as-prepared aerogels and xerogels were carbonized at 800°C under an argon gas flow for 5 h and cooled down naturally to room temperature. The obtained products were washed by 3 M hydrochloric acid three times to remove residual Al component. Then the aerogel derived carbon material, MOA-C, was obtained. The xerogel derived carbon was produced through further activation by KOH. Specifically, acid washed carbon product from xerogel precursor was mixed with KOH at the weight ratio of 1 : 4, then the mixture was heated at 700°C for 1 h under argon, followed by 3 M hydrochloric acid wash and deionized water wash. The obtained sample was named as MOX-C. MOX-C/S and MOA-C/S composites were prepared by a melt-diffusion strategy. The same weight of carbon products obtained above and sulfur were ground together and placed in a sealed vessel. Then the vessel was heated at 155°C for 12 h and 300°C for another 12 h before cooling down to room temperature naturally.

Characterization. PXRD patterns were recorded by Bruker D8 Advanced diffractometer at 40 KV and 40 mA, using Cu Kα radiation (λ = 1.5406 Å). Raman spectra were measured by Renishaw inVia microscope with an excitation wavelength of 532 nm. Thermogravimetric analyses (TGA) were performed on a TA Instruments SDT Q600 analyzer under a nitrogen flow with the heating rate of 5°C min^{-1}. Nitrogen sorption measurements were carried out with a Quantachrome Autosorb-IQ gas adsorption analyzer at 77 K. Prior to the sorption tests, samples were degassed under dynamic vacuum at 150°C for 5 h. For the C/S samples, they were degassed at room temperature due to the low melting point of sulfur (115°C). The BET surface areas were calculated from the adsorption data. The pore volumes were determined from the adsorbed amount at the relative pressure of 0.995. Pore size distributions were fitted by the Quenched Solid Density Functional Theory (QSDFT) using the desorption branch. The microstructures of the samples were investigated using a scanning electron microscope (SEM, Hitachi S-4800) and a transmission electron microscope (TEM, FEI Tecnai T20). Elemental mapping was performed on an energy dispersive X-ray spectroscope (EDS, Bruker Quantax) attached to the SEM.

H_2/CO_2/CH_4 sorption. H_2 sorption experiments were conducted by the Quantachrome Autosorb-IQ gas adsorption analyzer at 77 K. CO_2 and CH_4 sorption measurements were also carried out with the same instrument at 273 K. Prior to the sorption tests, samples were degassed under dynamic vacuum at 150°C for 5 h.

Electrochemical test. The working electrodes were comprised of 80 wt% C/S composite, 10 wt% Super P carbon and 10 wt% poly tetra fluoro ethylene (PTFE). The cathode materials were slurry-cast from isopropanol to a stainless steel foil and dried at 60°C for 12 h. For the MOX-C derived working electrode, the weight was 4.144 mg. For the case of MOA-C, the weight of the electrode was 4.088 mg. The coin cells were then assembled in an argon filled glove-box as follows: C/S composite as the test electrode, lithium metal foil as the counter electrode , 1 M LiTFSI solution in 1,3-dioxolane (DOL) and 1,2-dimethoxyetahne (DME) (1 : 1 volume ratio) as the electrolyte and Whatman GF/D borosilicate glass-fiber sheets as the separator. Coin

cells were tested at a current density of 400 mAg^{-1} within a voltage range of 1.0–3.0 V vs Li/Li^+ using Neware battery test system.

1. Schlapbach, L. & Züttel, A. Hydrogen-storage materials for mobile applications. *Nature* **414**, 353–358 (2001).
2. Wang, H. L., Gao, Q. M. & Hu, J. High Hydrogen Storage Capacity of Porous Carbons Prepared by Using Activated Carbon. *J. Am. Chem. Soc.* **131**, 7016–7022 (2009).
3. Li, L., Quinlivan, P. A. & Knappe, D. R. U. Effects of activated carbon surface chemistry and pore structure on the adsorption of organic contaminants from aqueous solution. *Carbon* **40**, 2085–2100 (2002).
4. Burke, A. Ultracapacitors: why, how, and where is the technology. *J. Power Sources* **91**, 37–50 (2000).
5. Wang, J., Zhang, X. B., Wang, Z. L., Wang, L. M. & Zhang, Y. Rhodium-nickel nanoparticles grown on graphene as highly efficient catalyst for complete decomposition of hydrous hydrazine at room temperature for chemical hydrogen storage. *Energy Environ. Sci.* **5**, 6885–6888 (2012).
6. Pekala, R. W. Organic aerogels from the polycondensation of resorcinol with formaldehyde. *J. Mater. Sci.* **24**, 3221–3227 (1989).
7. Tanaike, O., Hatori, H., Yamada, Y., Shiraishi, S. & Oya, A. Preparation and pore control of highly mesoporous carbon from defluorinated PTFE. *Carbon* **41**, 1759–1764 (2003).
8. Liang, C. D., Hong, K. L., Guiochon, G. A., Mays, J. W. & Dai, S. Synthesis of a Large-Scale Highly Ordered Porous Carbon Film by Self-Assembly of Block Copolymers. *Angew. Chem. Int. Ed.* **43**, 5785–5789 (2004).
9. Kyotani, T., Nagai, T., Inoue, S. & Tomita, A. Formation of New Type of Porous Carbon by Carbonization in Zeolite Nanochannels. *Chem. Mater.* **9**, 609–615 (1997).
10. Gui, X. C. *et al.* Carbon Nanotube Sponges. *Adv. Mater.* **22**, 617–621 (2010).
11. Numao, S., Judai, K., Nishijo, J., Mizuuchi, K. & Nishi, N. Synthesis and characterization of mesoporous carbon nano-dendrites with graphitic ultra-thin walls and their application to supercapacitor electrodes. *Carbon* **47**, 306–312 (2009).
12. Ahmadpour, A. & Do, D. D. The preparation of active carbons from coal by chemical and physical activation. *Carbon* **34**, 471–479 (1996).
13. Yu, C. Z., Fan, J., Tian, B. Z., Zhao, D. Y. & Stucky, G. D. High-Yield Synthesis of Periodic Mesoporous Silica Rods and Their Replication to Mesoporous Carbon Rods. *Adv. Mater.* **14**, 1742–1745 (2002).
14. Liu, B., Shioyama, H., Akita, T. & Xu, Q. Metal-Organic Framework as a Template for Porous Carbon Synthesis. *J. Am. Chem. Soc.* **130**, 5390–5391 (2008).
15. Yuan, D. S., Chen, J. X., Tan, S. X., Xia, N. N. & Liu, Y. L. Worm-like mesoporous carbon synthesized from metal-organic coordination polymers for supercapacitors. *Electrochem. Commun.* **11**, 1191–1194 (2009).
16. Liu, B., Shioyama, H., Jiang, H. L., Zhang, X. B. & Xu, Q. Metal-organic framework (MOF) as a template for syntheses of nanoporous carbons as electrode materials for supercapacitor. *Carbon* **48**, 456–463 (2010).
17. Hu, J., Wang, H. L., Gao, Q. M. & Guo, H. L. Porous carbons prepared by using metal-organic framework as the precursor for supercapacitors. *Carbon* **48**, 3599–3606 (2010).
18. Jiang, H. L. *et al.* From Metal-Organic Framework to Nanoporous Carbon: Toward a Very High Surface Area and Hydrogen Uptake. *J. Am. Chem. Soc.* **133**, 11854–11857 (2011).
19. Hu, M. *et al.* Direct synthesis of nanoporous carbon nitride fibers using Al-based porous coordination polymers (Al-PCPs). *Chem. Commun.* **47**, 8124–8126 (2011).
20. Radhakrishnan, L. *et al.* Preparation of Microporous Carbon Fibers through Carbonization of Al-Based Porous Coordination Polymer (Al-PCP) with Furfuryl Alcohol. *Chem. Mater.* **23**, 1225–1231 (2011).
21. Almasoudi, A. & Mokaya, R. Preparation and hydrogen storage capacity of templated and activated carbons nanocast from commercially available zeolitic imidazolate framework. *J. Mater. Chem.* **22**, 146–152 (2012).
22. Yang, S. J. *et al.* MOF-Derived Hierarchically Porous Carbon with Exceptional Porosity and Hydrogen Storage Capacity. *Chem. Mater.* **24**, 464–470 (2012).
23. Hu, M. *et al.* Direct Carbonization of Al-Based Porous Coordination Polymer for Synthesis of Nanoporous Carbon. *J. Am. Chem. Soc.* **134**, 2864–2867 (2012).
24. Chaikittisilp, W. *et al.* Nanoporous carbons through direct carbonization of a zeolitic imidazolate framework for supercapacitor electrodes. *Chem. Commun.* **48**, 7259–7261 (2012).
25. Lim, S. *et al.* Porous carbon materials with a controllable surface area synthesized from metal-organic frameworks. *Chem. Commun.* **48**, 7447–7449 (2012).
26. Pachfule, P., Biswal, B. P. & Banerjee, R. Control of Porosity by Using Isoreticular Zeolitic Imidazolate Frameworks (IRZIFs) as a Template for Porous Carbon Synthesis. *Chem. Eur. J.* **18**, 11399–11408 (2012).
27. Liu, B. *et al.* Converting cobalt oxide subunits in cobalt metal-organic framework into agglomerated Co_3O_4 nanoparticles as an electrode material for lithium ion battery. *J. Power Sources* **195**, 857–861 (2010).
28. Zhang, L., Wu, H. B., Madhavi, S., Hng, H. H. & Lou, X. W. Formation of Fe_2O_3 Microboxes with Hierarchical Shell Structures from Metal-Organic Frameworks and Their Lithium Storage Properties. *J. Am. Chem. Soc.* **134**, 17388–17391 (2012).
29. Xu, X. D., Cao, R. G., Jeong, S. & Cho, J. Spindle-like Mesoporous α-Fe_2O_3 Anode Material Prepared from MOF Template for High-Rate Lithium Batteries. *Nano Lett.* **12**, 4988–4991 (2012).
30. Li, S. L. & Xu, Q. Metal-organic frameworks as platforms for clean energy. *Energy Environ. Sci.* DOI: 10.1039/C3EE40507A (2013).
31. Eddaoudi, M. *et al.* Systematic Design of Pore Size and Functionality in Isoreticular MOFs and Their Application in Methane Storage. *Science* **295**, 469–472 (2002).
32. Gaab, M., Trukhan, N., Maurer, S., Gummaraju, R. & Müller, U. The progression of Al-based metal-organic frameworks-From academic research to industrial production and applications. *Microporous Mesoporous Mater.* **157**, 131–136 (2012).
33. Piepenbrock, M. O. M., Lloyd, G. O., Clarke, N. & Steed, J. W. Metal- and Anion-Binding Supramolecular Gels. *Chem. Rev.* **110**, 1960–2004 (2010).
34. Lloyd, G. O. & Steed, J. W. Anion-tuning of supramolecular gel properties. *Nat. Chem.* **1**, 437–442 (2009).
35. Hu, Y. L., Fan, Y. F., Huang, Z. L., Song, C. Y. & Li, G. K. In situ fabrication of metal-organic hybrid gels in a capillary for online enrichment of trace analytes in aqueous samples. *Chem. Commun.* **48**, 3966–3968 (2012).
36. Fellinger, T. P., White, R. J., Titirici, M. M. & Antonietti, M. Borax-Mediated Formation of Carbon Aerogels From Glucose. *Adv. Funct. Mater.* **22**, 3254–3260 (2012).
37. Aegerter, M. A., Leventis, N. & Koebel, M. M. *Aerogels Handbook* (Springer-Verlag New York, 2011).
38. Matsuoka, K. *et al.* Extremely high microporosity and sharp pore size distribution of a large surface area carbon prepared in the nanochannels of zeolite Y. *Carbon* **43**, 876–879 (2005).
39. Hou, P. X., Yamazaki, T., Orikasa, H. & Kyotani, T. An easy method for the synthesis of ordered microporous carbons by the template technique. *Carbon* **43**, 2618–2641 (2005).
40. Li, Z. Q., Lu, C. J., Xia, Z. P., Zhou, Y. & Luo, Z. X-ray diffraction patterns of graphite and turbostratic carbon. *Carbon* **45**, 1686–1695 (2007).
41. Wang, X. S. *et al.* Enhancing H_2 Uptake by "Close-Packing" Alignment of Open Copper Sites in Metal-Organic Frameworks. *Angew. Chem.* **120**, 7373–7376 (2008).
42. Yushin, G., Dash, R., Jagiello, J., Fischer, J. E. & Gogotsi, Y. Carbide-Derived Carbons: Effect of Pore Size on Hydrogen Uptake and Heat of Adsorption. *Adv. Funct. Mater.* **16**, 2288–2293 (2006).
43. Sevilla, M., Foulston, R. & Mokaya, R. Superactivated carbide-derived carbons with high hydrogen storage capacity. *Energy Environ. Sci.* **3**, 223–227 (2010).
44. Akridge, J. R., Mikhaylik, Y. V. & White, N. Li/S fundamental chemistry and application to high-performance rechargeable batteries. *Solid State Ionics* **175**, 243–245 (2004).
45. Bruce, P. G., Freunberger, S. A., Hardwick, L. J. & Tarascon, J. M. Li-O_2 and Li-S batteries with high energy storage. *Nat. Mater.* **11**, 19–29 (2012).
46. Nishihara, H. & Kyotani, T. Templated Nanocarbons for Energy Storage. *Adv. Mater.* **24**, 4473–4498 (2012).

Acknowledgments

This work was supported by the National Basic Research Program of China No. 2009CB939902, National Natural Science Foundation of China 11175006, New Star Program of Beijing Committee of Science and Technology (2012004), the Ministry of education program for New Century Excellent Talents of China (NCET-11-0027), and Singapore-Peking University SPURc program.

Author contributions

W.X. and R.Q.Z. designed the experiments and co-wrote the paper. W.X. performed the experiments and analyzed date. B.Q. and D.G.X. performed electrochemical test. All authors contributed to results analysis and discussion.

Additional information

Supplementary information accompanies this paper at http://www.nature.com/scientificreports

Competing financial interests: The authors declare no competing financial interests.

How to cite this article: Xia, W., Qiu, B., Xia, D. & Zou, R. Facile preparation of hierarchically porous carbons from metal-organic gels and their application in energy storage. *Sci. Rep.* **3**, 1935; DOI:10.1038/srep01935 (2013).